Electrochemical and Solid-State Letters, **9** (6) A311-A314 (2006)
1099-0062/2006/9(6)/A311/4/$20.00 © The Electrochemical Society

Effect of Anisotropic Volume Change in Tin Phosphate Nanoparticle Anode Material with Mesocellular Foam Structure on Capacity Retention

Eunjin Kim,[a] Min Gyu Kim,[b] and Jaephil Cho[a,*,z]

[a]*Department of Applied Chemistry, Kumoh National Institute of Technology, Gumi, Korea*
[b]*Beamline Research Division, Pohang Accelerator Laboratory, Pohang University of Science and Technology, Pohang, Korea*

Tin phosphate nanoparticles within microcellular foams were prepared using a nonionic triblock copolymer surfactant P123. The annealed sample at 500°C showed the particle size of 50–200 nm, and the size of the mesocelluar foam was ranged from 4 to 20 nm. Due to the irregular porewall thickness and pore size of the annealed sample, the pore wall structure had completely collapsed after first cycle. As the number of cycles increased, metallic tin clusters grew in the lithium phosphate matrix, and uniformly dispersed tetragonal tin nanoparticles with a particle size of 3 nm were observed after 100 cycles. This indicated that tin clusters decomposed from tin phosphate expanded and contracted reversibly in the matrix without particle aggregation. This was well supported by the electrochemical data, and the capacity increased to from 285 to 520 mAh/g with no capacity fading.
 [DOI: 10.1149/1.2193082]

Manuscript submitted January 16, 2006; revised manuscript received February 21, 2006. Available electronically April 7, 2006.

It has been reported that metal-based anode materials undergo severe particle aggregation and subsequent pulverization during discharge and charge processes.[1-3] This inherent problem originates from the ~300% volume expansion during Li alloying and dealloying. In contrast to the metal hosts, lithium-metal alloys (Li_xM), have a highly ionic character, and are usually brittle.[2] Therefore, mechanical stress related to volume changes induces a rapid decay in mechanical stability. The electrode suffers from pulverization as well as from the consequent loss of electronic interparticle contact. To minimize the volume change, synthetic strategies such as, active-inactive metal alloys,[4-6] carbon coating on metal particles[7-9] and particle size control[2,10,11] have been suggested. Recently, we proposed the incorporation of mesoporous structures as a buffer layer in which the mesopore can alleviate the volume expansion of the pore wall frames during lithium alloying/dealloying.[12,13] Here, pore and pore wall sizes ranged from 2–3 nm and 1.5-2.5 nm, respectively, depending on the surfactant. Kim et al. investigated mesoporous tin phosphates with surfactant $CH_3(CH_2)_nN(CH_3)_3Br$, with different alkyl chain lengths (n = 11, 13, 15, and 17).[13] These types showed a relatively ordered hexagonal and cubic pore structure with a particle size >5 μm. However, this study found some capacity fading after 30 cycles even though capacity retention was superior to other metal-based anodes, indicating that partial pore structures collapse during cycling.

In contrast to SiO_2 that have various types of mesopore structures,[14-19] lithium reactive tin phosphate shows only two types of pore structures as described above.[20,21] This paper reports the synthesis and electrochemical properties of mesoporous tin phosphate with a nanometer-sized particle size ranging from 50 to 150 nm, which were prepared using a nonionic triblock copolymer surfactant $EO_{20}PO_{70}EO_{20}$ (EO = ethylene oxide, PO = propylene oxide). This material has a mesocelluar foam structure.

Experimental

Pluronic P123 (10 g, BASF) were dissolved in 40 mL of distilled water into which 8.8 g of H_3PO_4 had been previously added. SnF_2 (3 g) was then added. The solution was stirred at 30°C for 20 h, and transferred to an autoclave, followed by keeping it at 90°C for 2 days. The precipitates were filtered using water and acetone, and fired at 500°C for 5 h to remove the surfactant in air. The X-ray diffraction (XRD) patterns of the samples were obtained using a Rigaku DMax5500PC X-ray diffractometer with Cu Kα radiation. The nitrogen adsorption isotherms were obtained with Micrometrics ASAP 2020 system, and the samples were degassed for 24 h at 150°C before the measurements. Field-emission transmission electron microscopy (TEM) investigations were carried out using a JEOL 2100F FE-TEM, operating at 200 kV. For the electrochemical tests, the slurry was prepared by mixing the mesoporous tin phosphate, Super P carbon black, and a binder (polyvinylidene fluoride) in a weight ratio of 6:1:1. The electrolyte used was ethylene carbonate/diethylene carbonate (EC/DEC) with 1 M $LiPF_6$ salts. Lithium metal was used for a counter electrode.

Sn L III-edge X-ray absorption spectra (XAS) of butyl-capped Ge nanoparticle for the first discharge-charge process were taken on BL7C1 (Electrochemistry) beamline in a storage ring of 2.5 GeV with a ring current of 120–170 mA at the Pohang Light Source (PLS). Si(111) double crystal monochromator were employed to monochromatize the X-ray photon energy.

Results and Discussion

Figure 1 shows the XRD patterns of the as-prepared and annealed tin phosphates at 500°C for 5 h. Small-angle XRD patterns of both samples clearly show no diffraction peaks indicating either no mesoporous phase or the formation of disordered mesoporous phase. Wide angle XRD patterns show the formation of $Sn(HPO_4)_2 \cdot H_2O$ and $SnHPO_4$ phases before and after annealing,

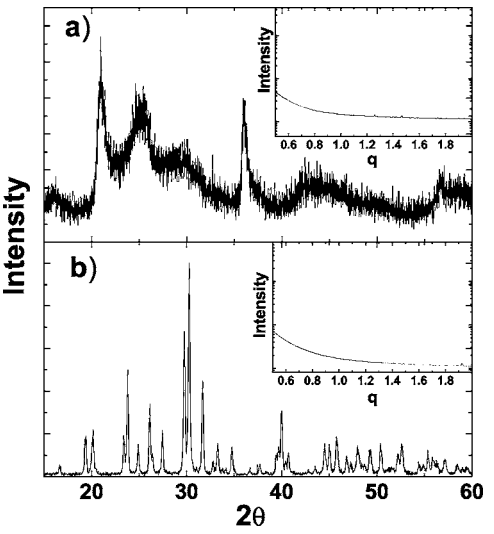

Figure 1. Wide and small angle (insets) XRD patterns of (a) as-prepared and (b) annealed tin phosphate at 500°C for 5 h ($q = 4\ \Pi\ \sin\theta/\lambda$).

* Electrochemical Society Active Member.
z E-mail: jpcho@kumoh.ac.kr

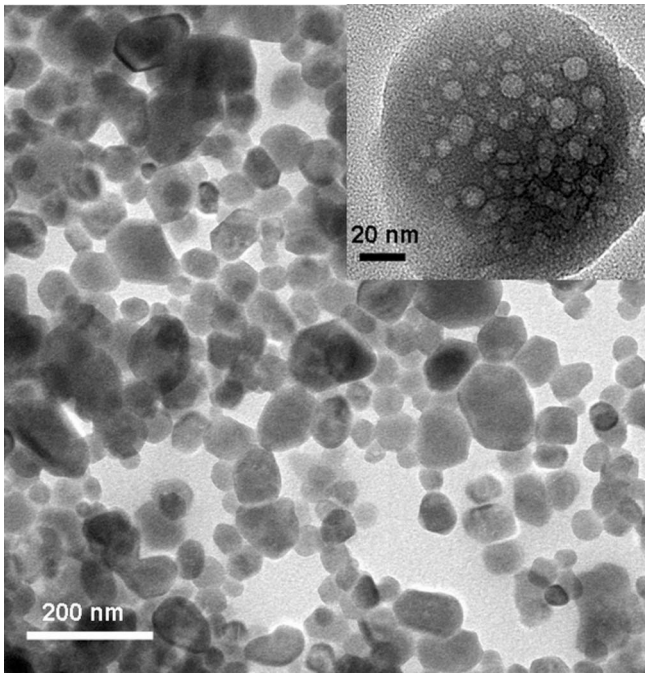

Figure 2. TEM images of the annealed tin phosphate at 500°C. The inset shows an expanded image of the particle.

respectively. Figure 2 shows the TEM image of the sample annealed at 500°C that was composed of 50 and 200 nm particles that were relatively well dispersed. Previously reported mesoporous tin phosphate had severely aggregated micrometer-sized particles, which were prepared using $CH_3(CH_2)_nN(CH_3)_3Br$.[13] TEM revealed the formation of mesocellular foamlike pore structure (Fig. 2, inset). This structure is similar to that of mesoporous SiO_2.[19] Accordingly, it is believed that the triblock copolymer surfactant acts as both a template for the mesostructure and a particle growth controller. Figure 3 presents that the annealed sample has a type IV N_2 adsorption/desoprtion isotherm with a type-H2 hysteresis loop, which is a consequence of the interconnectivity of a porous network with a wide distribution of pore sizes. The Barrett-Joyner-Halenda (BJH) method confirmed that the pore size was widely distributed between 20 and 4 nm, and the annealed sample has a high Brunauer-Emmett-Teller

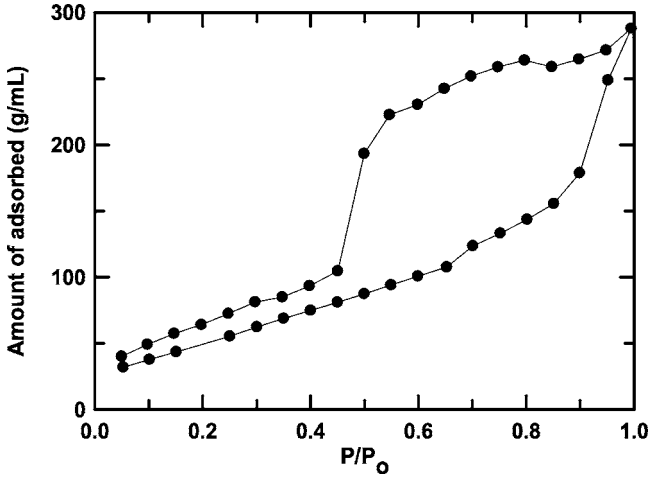

Figure 3. Nitrogen adsorption-desorption isotherms and pore-size distribution (inset) of the annealed sample. The sample was outgassed overnight at 150°C prior to analysis.

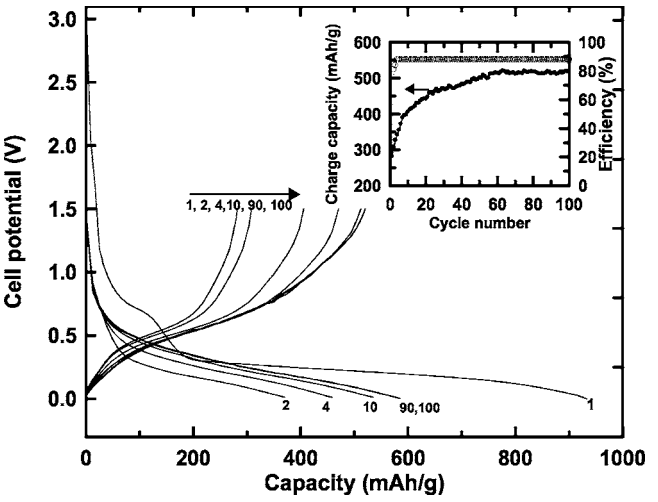

Figure 4. Voltage profiles of the annealed sample between 1.5 and 0 V after 1, 2, 4, 10, 40, 90, 100 cycles at the rate of 0.2 C (=80 mA/g), and the inset is a plot for the cycle life and cycling efficiency vs charge capacity.

surface area of 210 m^2/g. Because the pore walls are disordered and have a different pore wall thickness, the pores are expected to collapse during the lithium reactions, resulting in rapid capacity fading. It was previously reported that long range ordering of pore and regularity of pore wall thickness are key factors for retaining the reversible capacity retention, but the disordered mesoporous sample may not sustain volume expansion during the lithium reactions, resulting in the collapse of the pore walls.

Figure 4 shows the voltage profiles and cycle life of the annealed anode between 0 and 1.5 V at a rate of 0.2 C at up to 100 cycles. The first discharge and charge capacities were 920 and 285 mAh/g, respectively. However, the first charge capacity was gradually increased to 520 mAh/g after 100 cycles, and this behavior is completely different to mesoporous tin phosphate that showed gradual capacity fade.[12,13] A cycling efficiency of the sample was 30% for the first cycle but leveled off after 4 cycles, showing 88% out to 100 cycles. It was reported that $SnHPO_4$ could be reduced to active Sn and inactive Li_3PO_4 according to the following reaction[22]

$$SnHPO_4 + 7.7Li \rightarrow Li_{4.4}Sn + 1/2H_2 + Li_3PO_4 \qquad [1]$$

where Li_3PO_4 acts as the matrix phase for the tin particles. The gradual capacity increase may be related to the restricted electronic and Li ion conducting pathway between the tin atoms. Tin atoms are initially dispersed far apart in the matrix. Therefore, Li ions cannot diffuse readily from one tin atom to the next because the Li_3PO_4 matrix phase is a poor lithium ion conductor. In this condition, tin atoms separated in the matrix during initial cycles can have very

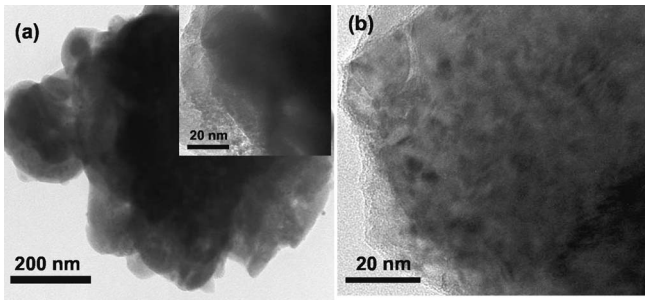

Figure 5. TEM images of (a) the annealed sample after 1 cycle (charged sample at 1.5 V; the inset is its expanded image) and (b) the annealed sample after 30 cycles (charged sample at 1.5 V).

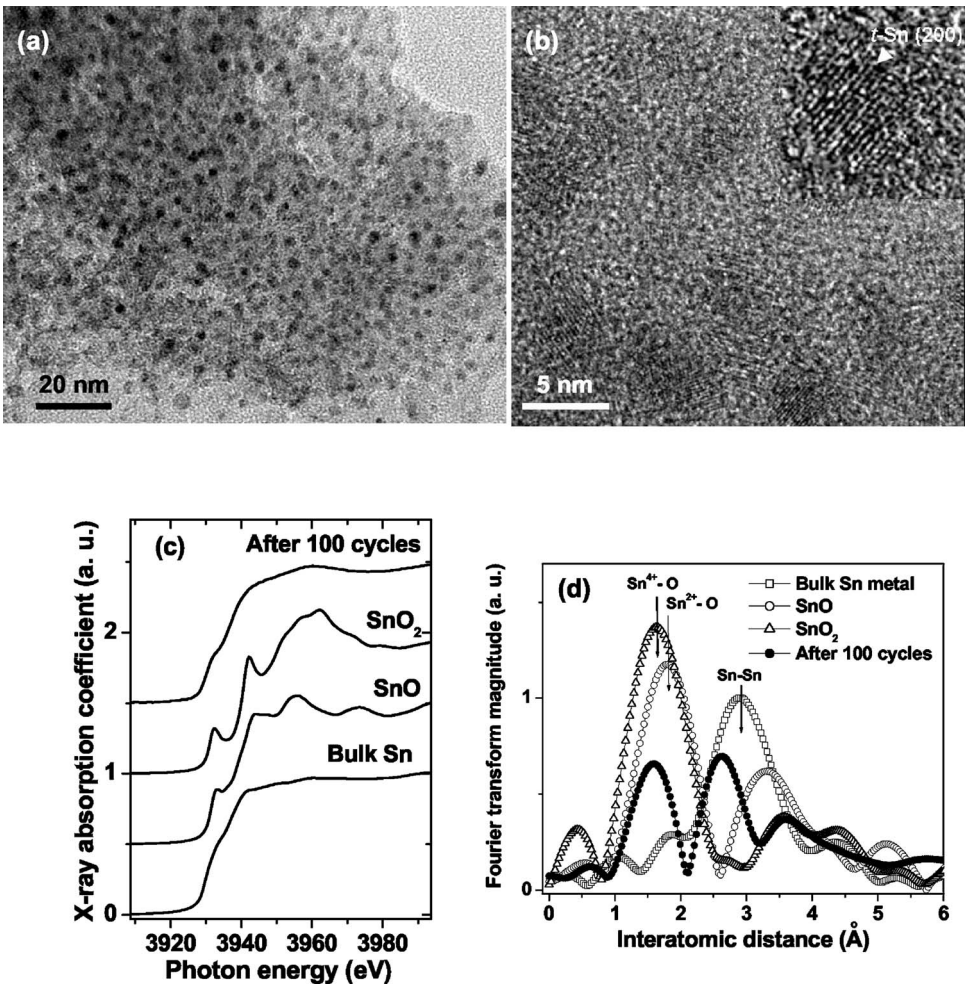

Figure 6. TEM images of the annealed sample (a) after 100 cycles (charged sample at 1.5 V) and (b) its magnified image. (c) normalized Sn L_{III}-edge XANES features of 100 cycled electrode and their corresponding FT magnitudes. (d) Sn L_{III}-edge k^3-weighted EXAFS spectra of the 100 cycled electrode, compared with those of bulk metallic Sn, SnO, and SnO_2 reference materials. For clarity, FT peak features of SnO and SnO_2 are plotted with half intensity.

limited lithium and electronic conductivity. However, once the tin moves over a greater distance to aggregate to a certain size, the distance between the Sn clusters becomes enough short to produce percolation pathways for the conduction.

To investigate the change in morphology of the sample during cycling, TEM images of the first, 30th, and 100th cycled samples after charging were compared (Fig. 5 and 6). After the first cycle, the disordered pores had completely disappeared, indicating that pores had collapsed. This is believed to be due to anisotropic volume contraction/expansion as a result of the different porewall thickness and random pore distribution. This is evidence of the small size of the tin clusters, probably consisting of only a few atoms that form after the first cycle. After 30 cycles, ~3 nm sized particles were observed in the Li_3PO_4 matrix, indicating that tin aggregated into the small clusters in the matrix. After 100 cycles, there were many Sn clusters with a uniform particle size of ~3 nm uniformly dispersed in the matrix, as shown in Fig. 6a. In particular, (200) lattice fringe of tetragonal tetragonal-Sn in Fig. 6b gives a direct evidence of formation of crystalline tin nanoparticles. This fact can be also proved with overall Sn metallic characteristics of Sn L_{III}-edge X-ray absorption near edge structure (XANES) and extended X-ray absorption fine structure (EXAFS) spectra, as shown in Fig. 6c and d. Tin oxides, SnO and SnO_2, show typical Fourier transform (FT) peaks of Sn-O bonding at 1.80 Å for Sn^{2+}-O and at 1.63 Å for Sn^{4+}-O, respectively, while bulk Sn metal gives a FT peak of Sn-Sn metallic bonding at about 2.8 Å. For the 100th cycled electrode, Sn-Sn FT peak is observed at about 2.6 Å, shorter than that of bulk Sn metal, indicating the size effect of the Sn nanoparticles. As a spectroscopic result, the electrode exhibits overall peak feature of Sn metallic state.

Note that the initial Sn size is constant even after 100 cycles, suggesting that the distance between tin clusters is unchanged, and the change in the volume of the tin clusters is reversible. Although further work is needed to determine the capacity retention mechanism, the 3 nm sized particles did not grow into larger particles during electrochemical cycling. This fact can be supported with an earlier study by Kim et al. that the critical size of metal-based anode materials for ensuring no capacity fading was ~3 nm.[23]

Conclusion

A mesocellular pore structure in tin phosphate nanoparticles completely collapsed during the lithium reactions, which was associated with a change in the anisotropic volume. However, the electrochemical cycling results showed no capacity fading even after 100 cycles, accompanied by gradual capacity increase out to 60 cycles, after which it leveled off. This was due to the fact that tin clusters did not grow into larger clusters and stopped their growth at ~3 nm. In addition, 3 nm sized tin nanoparticles were uniformly dispersed in the Li_3PO_4 matrix after 100 cycles.

Acknowledgments

The authors acknowledge the Pohang Light Source (PLS) for the XAS measurement. The experiments at the PLS were supported in part by Korea MOST and POSTECH. This work was supported by the Korea Research Foundation Grant funded by the Korean Government (MOEHRD) [C00230 (R05-2004-000-10029-0)]. Partial support from the Basic Research Program R01–2004–10173–0 of KOSEF is also acknowledged.

The Kumoh National Institute of Technology assisted in meeting the publication costs of this article.

References

1. I. A. Courteny and J. R. Dahn, *J. Electrochem. Soc.*, **144**, 2045 (1997).
2. M. Winter and J. O. Besenhard, *Electrochim. Acta*, **45**, 31 (1999).
3. M. Wachtler, J. O. Besenhard, and M. Winter, *J. Power Sources*, **94**, 189 (2001).
4. O. Mao, R. A. Dunlap, and J. R. Dahn, *J. Electrochem. Soc.*, **146**, 405 (1999).
5. K. D. Kepler, J. T. Vaughey, and M. M. Thackeray, *Electrochem. Solid-State Lett.*, **2**, 307 (1999).
6. K. C. Hewitt, L. Y. Bealieu, and J. R. Dahn, *J. Electrochem. Soc.*, **148**, A402 (2001).
7. I.-S. Kim, G. E. Blomgren, and P. N. Kumta, *Electrochem. Solid-State Lett.*, **7**, A44 (2004).
8. M. Noh, Y. Kwon, H. Lee, J. Cho, Y. Kim, and M. G. Kim, *Chem. Mater.*, **17**, 1926 (2005).
9. H. Kim, J. Choi, H.-J. Sohn, and T. Kang, *J. Electrochem. Soc.*, **146**, 4401 (1999).
10. M. Noh, Y. Kim, M. G. Kim, H. Lee, Y. Kwon, Y. Y. Lee, and J. Cho, *Chem. Mater.*, **17**, 3320 (2005).
11. Y. Kwon, M. G. Kim, Y. Kim, Y. Lee, and J. Cho, *Electrochem. Solid-State Lett.*, **9**, A34 (2006).
12. E. Kim, D. Son, T.-G. Kim, J. Cho, B. Park, K. S. Ryu, and S. H. Chang, *Angew. Chem., Int. Ed.*, **43**, 5987 (2004).
13. E. Kim, M. G. Kim, Y. Kim, and J. Cho, *Electrochem. Solid-State Lett.*, **8**, A452 (2005).
14. K. Kuzuki, K. Ikari, and H. Imai, *J. Am. Chem. Soc.*, **126**, 462 (2004).
15. Q. Cai, Z. S. Luo, W. Q. Pang, Y. W. Fan, X.-H. Chen, and F.-Z. Cui, *Chem. Mater.*, **13**, 258 (2001).
16. R. I. Nooney, D. Thirunavukkarasu, Y. Chen, R. Josephs, and A. E. Ostafin, *Chem. Mater.*, **14**, 4721 (2002).
17. W. Zhao and Q. Li, *Chem. Mater.*, **15**, 4160 (2003).
18. D. Grosso, E. L. Crepaldi, B. Charleux, and C. Sanchez, *Adv. Funct. Mater.*, **13**, 37 (2003).
19. Y. Han and J. Y. Ying, *Angew. Chem., Int. Ed.*, **44**, 288 (2005).
20. C. Serre, A. Auroux, A. Gervasini, M. Hervieu, and G. Ferey, *Angew. Chem., Int. Ed.*, **41**, 1594 (2002).
21. T. Kimura, Y. Suguhara, and K. Kuroda, *Chem. Commun. (Cambridge)*, **1998**, 559.
22. M. L. E. Moubtassim, J. I. Corredor, J. L. Tirado, and C. P. Vicente, *Electrochim. Acta* **47**, 489 (2001).
23. C. Kim, C. M. Noh, M. Choi, J. Cho, and B. Park, *Chem. Mater.*, **17**, 3297 (2005).